Astron. Astrophys. 317, 223–231 (1997)

ASTRONOMY
AND
ASTROPHYSICS

The impulsive phase of the arcade flare of 28 June 1992, 14:24 UT

M. Tomczak

Astronomical Institute, Wrocław University, Kopernika 11, PL-51-622 Wrocław, Poland (e-mail: tomczak@astro.uni.wroc.pl)

Received 5 January 1996 / Accepted 22 April 1996

Abstract. *Yohkoh* Soft X–Ray Telescope and Hard X–Ray Telescope observations of an M 1.6 limb flare of 28 June 1992, 14:24 UT have been analyzed. The flare occurred in a magnetic arcade. Basic observational characteristics of soft and hard X–ray emission for this flare have been compared. Excellent examples of impulsive soft X–ray brightenings have been found. Velocities of the chromospheric evaporation have been estimated directly from the SXT images. Derived values 460–750 km s^{-1} are consistent with previous spectral observations, but greater than results of standard theoretical models. Two separated places of simultanous energy release at the top of the arcade have been found. These places showed a different behaviour but clear connection. The location of the low-lying hard X–ray emission sources above the footpoints of the arcade has been explained as a result of a magnetic field convergence. The importance of the impulsive soft X–ray brightenings in investigation of the precipitation of non-thermal electrons has been emphasized.

Key words: Sun: corona – Sun: flares – Sun: X–rays, gamma rays

1. Introduction

Investigation of the spatial structures of solar flares is still fruitfully in progress. The Japanese satellite *Yohkoh* (Ogawara et al. 1991) has been providing plenty of new data from two imaging instruments: Hard X–Ray Telescope (HXT) and Soft X–Ray Telescope (SXT). The HXT (Kosugi et al. 1991) records images in four energy bands, 14–23–33–53–93 keV, with an angular resolution $\geq$ 5 arc sec and a time resolution up to 0.5 s. The SXT (Tsuneta et al. 1991) produces images using five broadband filters over a range of energies between 0.28 and 4 keV, with a pixel size 2.45 arc sec. The time resolution is 2 s per image, or 10 s per repetition of any particular filter.

One of the most important results of *Yohkoh* mission is a discovery of impulsive soft X–ray brightenings during an impulsive phase of flares (Hudson 1994). First report (Strong et al. 1994) showed that such kind of emission is located at the "footpoints" i.e. *at the entrance of magnetic coronal structures into the lower part of the solar atmosphere*. Authors emphasized good temporal and spatial correlations between soft X–ray brightenings and hard X–ray bursts. Their survey of 14 flares suggested that almost each flare with a well-observed impulsive phase shows impulsive soft X–ray brightenings.

A physical interpretation connects the impulsive soft X–ray brightenings with the chromospheric evaporation model (Hudson et al. 1994). Observed brightenings have relatively low-temperature (less than 10 MK) thermal spectra. The authors concluded that such emission *comes from material heated by precipitating electrons at loop footpoints and evaporating from the deeper atmosphere into the flaring flux tube*.

The 28 June 1992, 14:24 UT flare gave an excellent opportunity for an analysis of the impulsive soft X–ray brightenings in a long-duration arcade event. First, it was a limb flare which allowed me to study its vertical structure. Second, this flare had a well-marked impulsive phase that consisted of several distinct hard X–ray bursts. Third, during the whole impulsive phase the SXT provided a high time resolution sequence of unsaturated images.

In Sect. 2 I present an analysis of the SXT data: a morphology of a flare magnetic structure, details of the impulsive soft X–ray brightenings. Results of HXT image synthesis are given in Sect. 3. A comparison between the SXT and the HXT images is described in Sect. 4. In Sect. 5 I interpret and discuss the reported observations. In Sect. 6 I summarize the basic conclusions of my paper.

2. The SXT observations

The analysed flare (GOES class M 1.6) occurred in NOAA Active Region 7216 on the east limb, the N15 latitude. The maximum of this flare in the GOES 1–8 Å band was reached at about 14:24 UT. The flare occurred in an arcade of magnetic loops that was observed from one side (Tomczak 1994).

I identified at least seven legs that foopoints are labelled F1, F2, ..., F7 respectively, in Fig. 1a. The tops of the loops converged into two places K1 and K2. These places became the brightest in the whole arcade after the impulsive phase (Figs. 1c–d). Such a scenario resembles the evolution described first by Acton et al. (1992) and confirmed in the case of arcade flares by Feldman et al. (1995). The northern loop-top emission

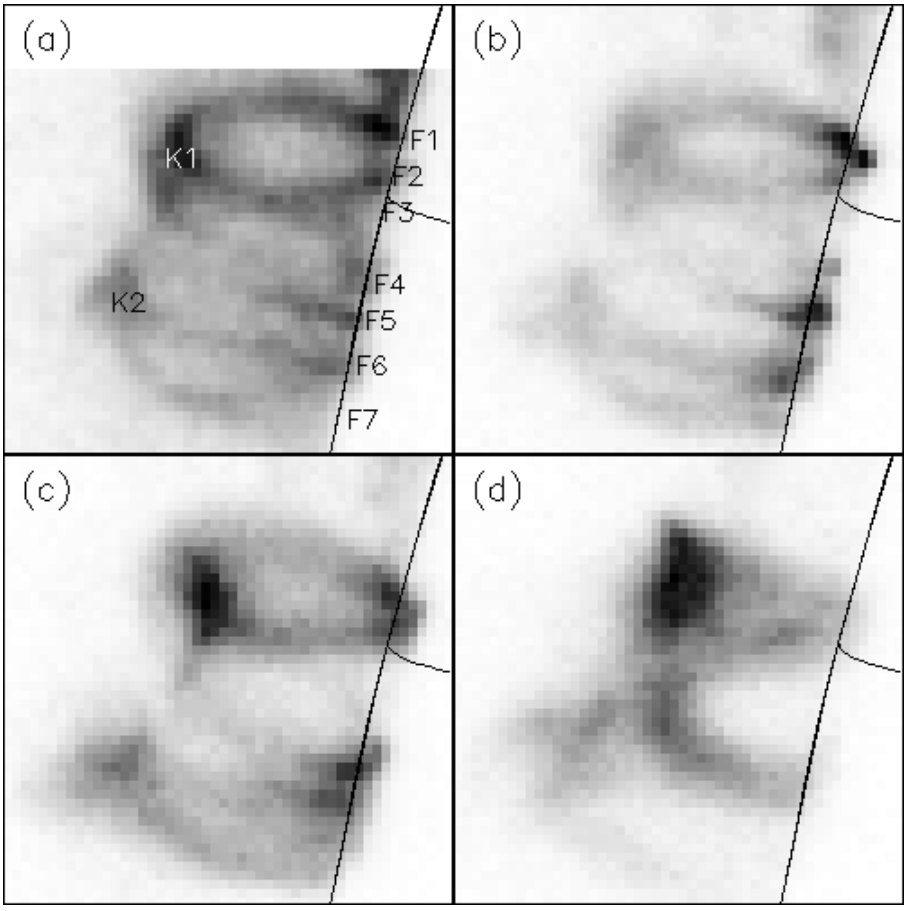

Fig. 1a–d. A mosaic of four SXT/Al12 images illustrating the evolution of the 28 June 1992, 14:24 UT flare. Each image consists of 50 x 50 2.45 arc sec pixels and has its own scale of brightness based on the brightest pixel. North is at the top, east – on the left. Continuous curves represent the solar east limb and the latitude N15. **a** An image made at 13:52:16 UT, about 3 minutes before the beginning of the impulsive phase. The more characteristic features of the flare morphology have been marked. **b** A frame taken at 13:56:30 UT, just before the time of the strongest hard X-ray burst. **c** The image recorded at 14:01:08 UT, on the rising phase of the flare after the impulsive phase. **d** The frame made at 14:25:08 UT, during a soft X–ray maximum.

kernel K1 was definitely brighter than the southern kernel K2 and had five legs (1–5) mostly brighter than the legs 6 and 7 coming out of kernel K2.

The footpoints of two legs of the arcade (F2 and F7) seemed to be partly obscured by the limb, and five others footpoints were visible on the disk. This confirmed an exactly limb location of the loop-top emission kernels and allowed me to obtain their heights precisely. Also the Hα flare history of the AR 7216 shown that the passage through the E90 longitude occured during the period of the analysed flare. At the beginning of the flare the kernel K2 was about 4.8×10^4 km height, and the kernel K1 was about 4.3×10^4 km height. During the flare evolution I observed a gradual decrease of the height of the kernel K1. Its height around the maximum of soft X–ray intensity was about 3.2×10^4 km only. During the whole flare evolution the height of the kernel K2 was approximately constant.

The impulsive phase of the investigated flare lasted about five minutes between 13:55 and 14:00 UT. The 25–50 keV light curve recorded by the Burst and Transient Source Experiment (BATSE) instrument (Fishman et al. 1989) onboard the Compton Gamma Ray Observatory (CGRO) showed three main and several weaker bursts (Fig. 2a). The main bursts reached their peaks at 13:55:40 (I), 13:56:47 (II) and 13:57:40 UT (III) respectively.

During the impulsive phase each footpoint of the identified legs showed an impulsive soft X–ray brightening (Fig. 1b). This effect was most prominent in the Al12 filter. Using images in this filter, the time history of the brightness of each pixel during the impulsive phase was plotted (Fig. 3). In each of these light curves all statistically significant peaks were selected. I have taken the time of such a peak as the central point of a time period when the light curve was above a low error boundary of a peak of the selected part of the light curve.

Figure 2b presents a histogram showing the number of pixels in the investigated footpoints reaching a peak at a given time. Five peaks can be clearly identified. Three of them correspond

Table 1. Number of SXT/Al12 pixels reaching the peak of brightness

Footpoint	Burst				
	I	E	II	III	W
F1	10	1	23[a]	18[a]	–
F2	6	–	–	–	–
F3	1	–	9	2	–
F4	6	–	2	2	9
F5	–	12[a]	7	–	–
F6	8	1	7	4	1
F7	–	–	4	–	–

[a] Time evolution

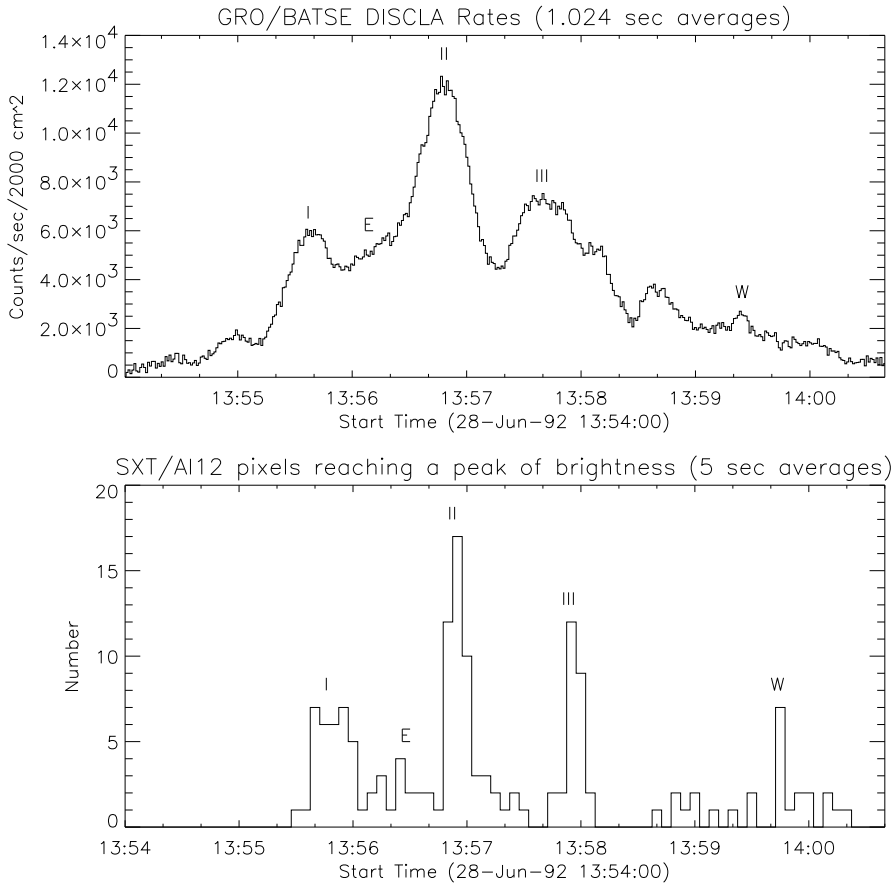

Fig. 2. a The CGRO/BATSE 25–50 keV light curve of the 28 June 1992, 14:24 UT flare. Marked features (i.e. I, E, II, III, W) had a response in soft X–rays (see text for more details). **b** Time history of number of pixels reaching the peak of brightness during the impulsive phase on the SXT/Al12 images.

to the main hard X–ray bursts I, II and III, one corresponds to the enhancement on a rise part of the burst II (E), and one – to the weak burst at 13:59:24 UT (W). The other weak hard X–ray bursts in Fig. 2a have no evident corresponding impulsive soft X–ray brightenings in Fig. 2b.

The basic behaviour of the impulsive soft X–ray brightenings of the 28 June 1992, 14:24 UT flare can be summarised as follows:

1. The individual footpoints had distinctly different light curves, as seen in Fig. 3. The number of pixels contributing from each footpoint to each peak in Fig. 2b is given in Tab. 1. Thus, Tab. 1 shows which footpoints respond to each hard X–ray burst. Only during the strongest hard X–ray burst II the impulsive soft X–ray brightenings were observed in almost every footpoint. Sometimes one footpoint reacted to a particular hard X–ray burst, e.g., footpoint F5 – to the burst E, and footpoint F4 – to the burst W.
2. There is a systematic delay of the peak of the soft X–ray brightenings with respect to the maximum of the hard X–ray bursts. Values of delay were between 5 and 35 s, for different hard X–ray bursts. Also, for a particular hard X–ray burst I observed a difference in the delay for the different footpoints, e.g. for burst II the average delay was 5, 7, 10 and 35 s for the footpoint F3, F1, F6 and F7 respectively.
3. In three cases I found a systematic trend: the moment of the impulsive soft X–ray brightening peak depended on the location in the leg – pixels located higher in the leg peaked later in time. This is a manifestation of chromospheric evaporation. I calculated the velocity of the evaporating plasma by fitting a straight line to the dependence of the peak time on the distance along the leg (Fig. 4). Derived velocities are 460 ± 60 km s^{-1} in the case of the E burst in the footpoint F5, 590 ± 95 km s^{-1} and 750 ± 180 km s^{-1} in the footpoint F1 during the II and III burst, respectively.
4. During the impulsive phase the footpoints were the brightest parts of the whole arcade in the soft X–rays. In a comparison to a pre-flare data (the Al12 image of 13:52:16 UT) the brightness of the footpoints increased at least by a factor of 5. In an extreme case of one pixel from the footpoint F1 during burst II, this increase was more than a factor of 50.
5. The temperature of the footpoints calculated from the SXT Be119 and Al12 filter ratio during the impulsive phase was rather low (6–9 MK), and nearly constant. Thus, the main reason of the increase in brightness was an increase of the emission measure due to plasma heating.

3. The HXT observations

I have calculated hard X–ray images for L (14–23 keV) and M1 (23–33 keV) channels during three main bursts, using the Maximum Entropy Method program written by T. Sakao (Sakao 1994; Morrison 1994). Higher energy HXT channels had in-

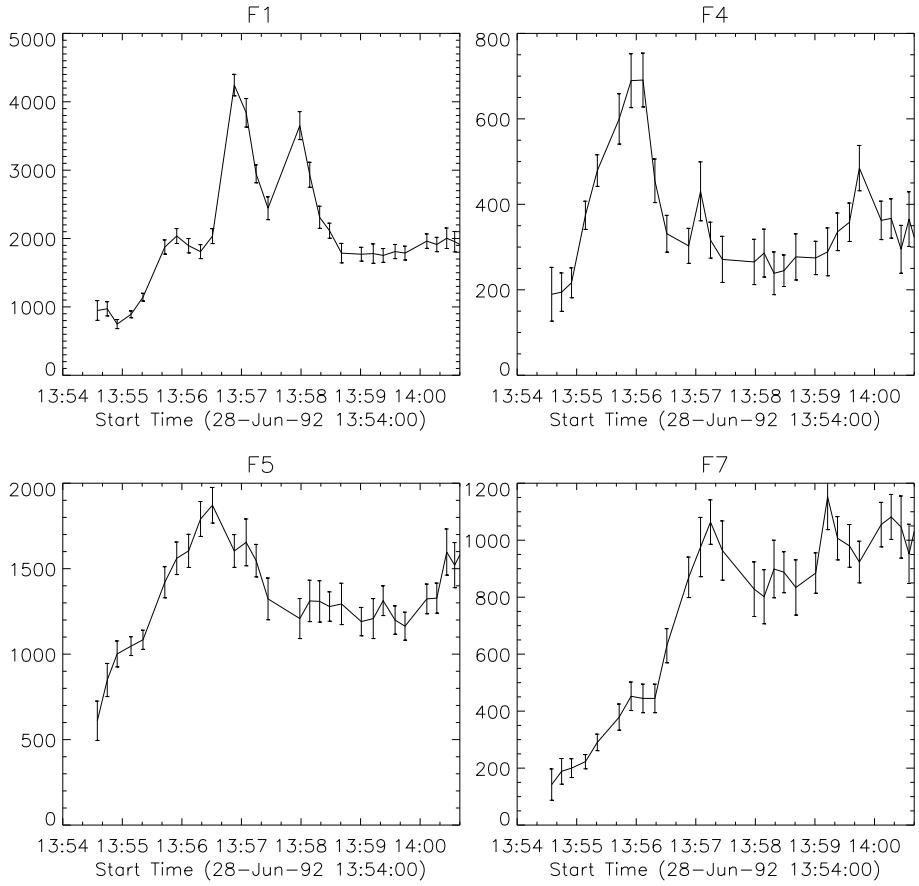

Fig. 3. The SXT/Al12 light curves (in DN s^{-1} units) for four representative pixels from the footpoints F1, F4, F5 and F7 during the impulsive phase.

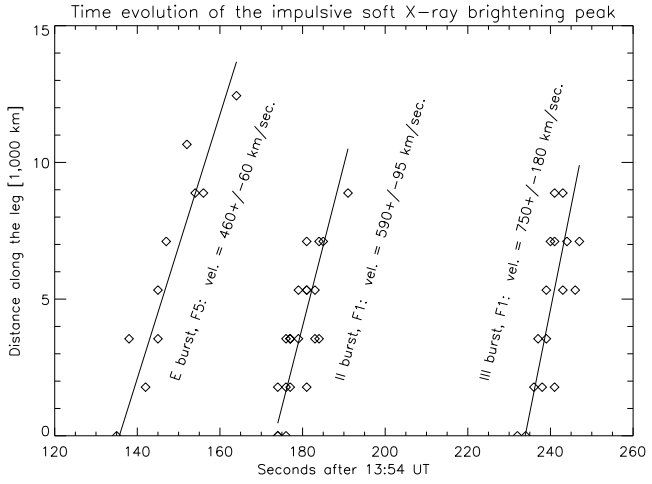

Fig. 4. Moment of the impulsive soft X–ray brightening peak versus distance along the leg measured from the SXT/Al12 images. A linear fit to the data is shown as a continuous line. An identification of the hard X–ray burst and the leg, and the value of the velocity are given.

sufficient number of counts to produce images. In the case of arcade flares such relatively soft hard X–ray spectra appear to occur very frequently (Tomczak 1994; Uchida 1995).

I identified four sources of hard X–ray emission (Fig. 5): two high-lying (H1, H2) and another two low-lying (H3, H4) sources. The strongest source, H1, had a horn-shape with a maximum in the middle. Sometimes I observed a second local maximum at the southern end of this source. The source H2 was relatively compact and had a round shape. The source H3 was clearly elongated. Occasionally it had a little compact component in the north-west direction seen in the channel M1 only. The source H4 consisted of two parts: an elongated southern and a compact northern part. The sources H3 and H4 had a tendency to connect with the source H1 in the channel L. Only the source H2 was separated throughout the whole impulsive phase.

Figure 6 presents light curves of the individual sources of hard X–ray emission in both channels and time evolution of the hardness ratio M1/L for each source. The source H1 was responsible for approximately half of the total hard X–ray emission during the whole impulsive phase. For the source H1, each of the main hard X–ray bursts (I, II, and III) had a clear peak featuring a temporary increase of the hardness ratio.

Source H2 I shared distinctly different behaviour. Each burst was smoothed. The peak of the burst I was not observed, and the peaks of bursts II and III were delayed by 20–30 s in a comparison to the H1 source. Also, the hardness ratio for the H2 source was definitely greater than for the other sources and the increase of the hardness ratio lasted during almost the whole duration of the bursts.

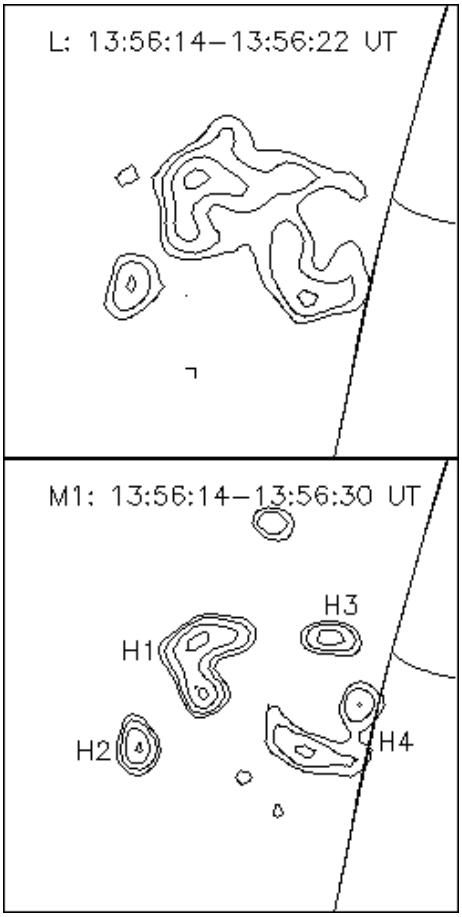

Fig. 5. Examples of hard X–ray images of the 28 June 1992, 14:24 UT flare. Channel number and periods of accumulation are shown. Contour levels are 78.4, 39.2, 19.6 and 11.8 % of the maximum intensity for each image. The scale and the orientation are the same as for the Fig. 1.

There was a clear similarity between the source H1 and the low-lying source H3 in their hard X–ray light curves and the evolution of the hardness ratio M1/L. Both sources had three distinct bursts, relatively early times of maximum, and short durations of the increase of the hardness ratio.

I also found similarities in the hard X–ray light curves and hardness ratio for the source H2 and the another low-lying source H4: the lack of burst I, later moments of peaks of bursts II and III, and a longer duration of the increase of the hardness ratio.

A common feature of all hard X–ray emission sources was a continuing decrease of the hardness ratio with time.

4. Comparison of SXT and HXT images

I carefully compared the HXT and SXT images. The accuracy of the overlay was about 1.5 arc sec. Figure 7 shows representative examples of the SXT/Al12 images recorded during the hard X–ray bursts II and III. I also overplotted contours of HXT emission in the channel L (left panels), emission in the channel M1 (middle panels) and a temperature map calculated according the filter ratio method (Hara et al. 1992; Morrison 1994) from the SXT Be119/Al12 filter ratio (right panels). For better statistics I calculated the temperature maps for 4.9 x 4.9 arc sec pixels.

The high-lying hard X–ray emission sources H1 and H2 coincided spatially quite well with the loop-top soft X–ray emission kernels K1 and K2 respectively. In particular, they had similar size and shape. Nevertheless, the brightest pixel of the H1 source was systematically shifted in the south-west direction, in a comparison to the brightest pixel of the K1 kernel. The shift was about 10 arc sec, on average. Approximately the same average value of shift but in the north-west direction was found for the H2 source relative to the K2 kernel.

A similar displacement was observed between the brightest pixel in the hard X–ray emission and the hottest pixel in the SXT temperature map in the case H2–K2. Better co-spatial agreement between HXT emission and SXT temperature map was found in the case H1–K1, where an average shift between the brightest pixel of the H1 kernel and the hottest pixel on the SXT temperature map was about twice lower i.e. 5 arc sec.

Such a relationship resembles other flares e.g. of 13 January 1992 (Masuda 1994), where the spatial correlation between hard X–ray emission and SXT temperature map was also better than the spatial correlation between hard X–rays and soft X–rays. An important difference is that in the case of 28 June 92, 14:24 UT flare, the area of the highest SXT temperature and the area of the maximum of hard X–ray emission were located approximately at the same height as the SXT loop-top emission kernels.

The low-lying hard X–ray emission sources H3 and H4 did not have distinct counterparts in the SXT images, where I did not observe any local maximum of the intensity distribution. An exception was the relatively weak, compact part of the H3 source, observed in channel M1 only, that covered fragments of the footpoint F1 – the brightest in soft X–rays. The elongated part of the H3 source coincided spatially with two unresolved legs (hereafter the legs 2+3), that connected the kernel K1 with the footpoints F2 and F3. The northern part of the H4 source coincided spatially with the lower portion of the leg 4. The southern part of the H4 source coincided with leg 5. The legs 6 and 7 that converge into the southern loop-top emission kernel K2 on the SXT images did not show any hard X–ray emission.

The low-lying hard X–ray emission sources also did not have any counterparts on the SXT temperature maps. The spatial distribution of temperature at the places of the arcade where I localised sources H3 and H4 showed a monotonic decrease from the loop-top emission kernels to the footpoints without any local maximum.

The footpoints of the arcade – the places of the impulsive soft X–ray brightenings – did not have counterparts in hard X–rays. Some legs (6 and 7) did not show hard X–ray emission at all, other legs (2+3, 4 and 5) had the maximum of hard X–ray emission sources located at significant heights: 1.3×10^4, 3.5×10^3, 1.1×10^4 km respectively, in average. The footpoints had up to 10 times less intense hard X–ray emission than the loop-top regions and several times less intense emission than the legs above the footpoints in both HXT channels L and M1.

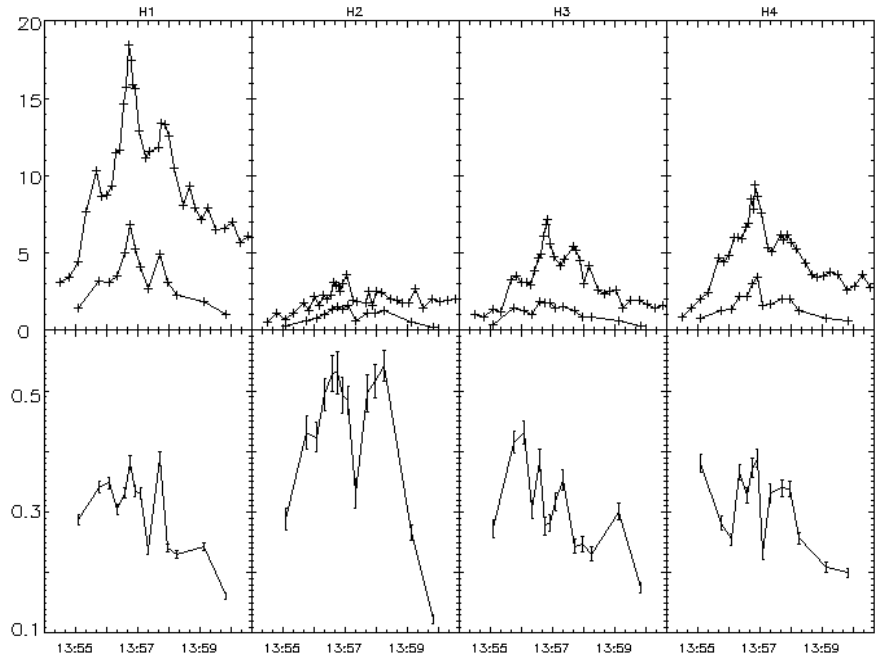

Fig. 6. Time evolution of the intensity in the channel L (upper panels, upper curves), in the channel M1 (upper panels, bottom curves) and the hardness ratio M1/L (bottom panels) for the individual hard X–ray emission sources. Intensities are in cts s^{-1} cm^{-2} units.

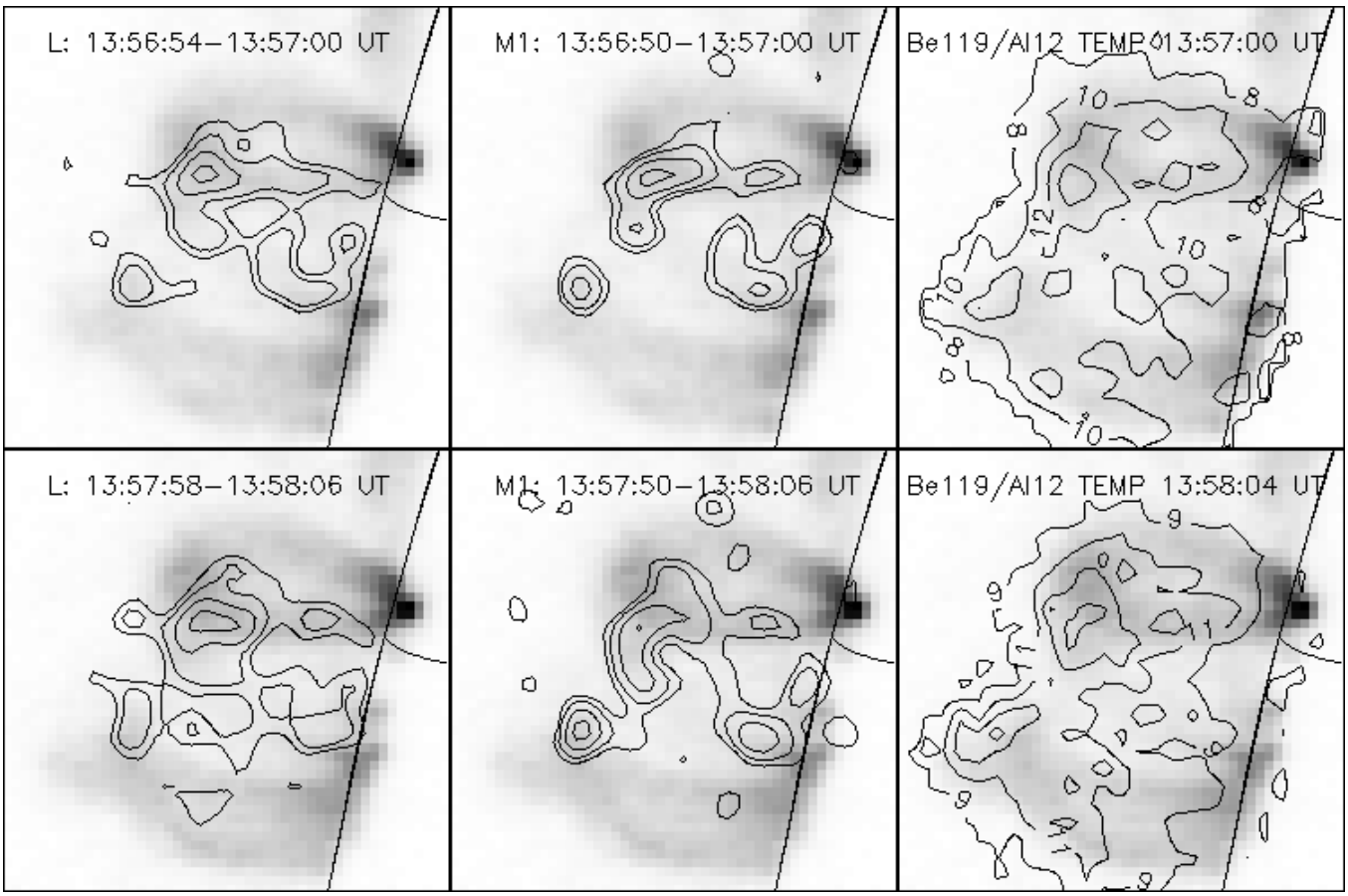

Fig. 7. Examples illustrating the spatial localisation of the SXT/Al12 images (gray scale) in a comparison to: the L images (left panels), the M1 images (middle panels) and the Be119/Al12 map temperature (right panels). The scale and the orientation are the same as for the Fig. 1. Contour levels of the hard X–ray images are the same as for the Fig. 5. Temperature units are 10^6 K. The interval between temperature contours is 2×10^6 K.

An exception was the footpoint F1, where on several images in the channel M1 I identified a small compact source of emission located in the area of the soft X–ray brightening.

5. Discussion

5.1. The high-lying hard X–ray emission sources

Jakimiec (1990) has shown that in order to heat and maintain a large amount of flare plasma at high temperature $T > 10$ MK, it is necessary that the plasma be turbulent and that the MHD turbulence is the most suitable for this. The turbulence will also accelerate a part of electrons to higher energies, say $E > 20$ keV by (1) acceleration in individual episodes of magnetic field reconnection or (2) stochastic Fermi acceleration (being also efficient for ions).

On this basis, in the paper of Jakimiec (1991) it has been argued that the flare energy release occurs in turbulent regions, which can be called "turbulent flare kernels". These kernels have been identified with the kernels of the soft and hard X–ray emission, as well as microwave emission (cf. also Jakimiec and Fludra 1991). These flare kernels are very well seen in *Yohkoh* SXT (e.g. Acton et al. 1992) and HXT images (Masuda 1994; Kosugi 1994 - so called *loop-top sources*) and can be investigated in some detail (Jakimiec et al. 1994).

The magnetic lines escaping from the turbulent kernels determine the magnetic flux tubes connecting the kernel with the chromosphere and they are seen as the "legs" in soft X–rays. The magnetic field is turbulent in the kernels and regular in the legs. Higher energy electrons accelerated within or near the edge of a kernel either get the open lines of force, escape to the flare legs and run to their footpoints, or they get into the irregular (tengled) magnetic field in the kernel giving rise to the hard X–ray bremsstrahlung emission from the kernels (Jakimiec 1991).

This scenario is in a very good agreement with the observations of the investigated flare, as well as with many other *Yohkoh* flares. During the impulsive phase the both sources H1 and H2 appears to be the sites of energy release in the arcade. In both places I observed simultanously two effects of the energy release: high-temperature plasma and bremsstrahlung from non-thermal electrons. High-temperature plasma was responsible for the strong increase of temperature and local maxima on the SXT temperature maps in the kernels K1 and K2 area throughout the impulsive phase. Values of the hardness ratio M1/L for the sources H1 and H2 suggest a power-law photon spectrum that is typical for non-thermal electrons. A power-law index γ during the impulsive phase was between 5.5–6.5 and 4.6–5.2 for the sources H1 and H2 respectively.

Masuda (1994) showed that impulsive loop-top hard X–ray sources can divided into two groups. The first group consists of the sources located inside the soft X–ray emission kernels having relatively soft spectra ($\gamma = 5.5$). Second group consists of the impulsive loop-top hard X–ray sources located higher than the soft X–ray emission kernel and having harder spectra ($\gamma = 1.3$–3.5). The sources H1 and H2 of the 28 June 1992, 14:24 UT had the features typical for the first Masuda type.

The observational characteristics suggested that the source H1/kernel K1 during the whole impulsive phase was the main place of the energy release in the arcade. The source H1/kernel K1 was distinctly brighter in soft and hard X–rays than the source H2/kernel K2 and had higher values of the SXT temperature. The relative contributions of the two effects of energy release in the high-lying sources varied. Around the peaks of the main hard X–ray bursts I observed the increase of amount of non-thermal electrons having the harder spectrum. The systematic decrease of the hardness ratio during the impulsive phase outside the bursts shows that the significance of the high-temperature plasma increased in time. The source H2 showed higher values of the hardness ratio M1/L and a prolonged increase of this ratio in a comparison to the source H1. It suggests that in this part of the arcade the relative contribution of non-thermal electrons was systematically higher than in the source H1.

Energy released during the impulsive phase could be transported along magnetic flux tubes having good magnetic connection with the kernels to other parts of the arcade in two forms: non-thermal electron beams and thermal conduction. The importance of the first energy transport mechanism is confirmed by the impulsive soft X–ray brightenings (Fig. 2). The SXT temperature maps illustrate the second energy transport mechanism (Fig. 7, right panels), where the spatial distribution of temperature resembls the shape of the arcade. Temperatures monotonically decrease from the kernels K1 and K2 to the footpoints along the magnetic flux tubes.

5.2. The low-lying hard X–ray emission sources

As a sample of the typical footpoint source in the impulsive phase according the recent classification by Kosugi (1994) I consider a small compact hard X–ray source observed sometimes in the footpoint F1 area in the channel M1 (Fig. 7).

The low-lying hard X–ray emission sources H3 and H4 cannot be considered as typical footpoint sources in the impulsive phase. First, they were too weak and too soft in a comparison to other described footpoint sources (Sakao 1994). Second, these sources were weaker than the H1 source and softer than the H2 source. Third, they were located several thousand kilometers above the footpoints. A more adequate name for such sources would be *the hard X–ray emission sources above footpoints*.

The H3 and H4 sources looked like the hard X–ray source located in a southern leg of a second loop of 6 February 1992 flare (Kosugi et al. 1994). The authors suggested that this loop had a relatively high value of electron density and that such feature was the basic reason of the atypical characteristics of the hard X–ray sources.

The 28 June 1992, 14:24 UT flare had a rather low electron density. During the impulsive phase the values of electron density in the arcade obtained from the SXT images estimated at about 1–2×10^{10} cm^{-3} for the kernels K1 and K2 and up to 4×10^{10} cm^{-3} in the case of the most prominent soft X–ray brightening. The mean free paths for electons of energies of the channel L and M1 are 1.2×10^{10} cm and 3.2×10^{10} cm respec-

tively. Thus, the electron density of the coronal part of the arcade was too low to stop non-thermal electron beams. Moreover, such an effect should depend on the energy: lower energy channel – higher position in the corona, but the heights of the sources H3 and H4 were the same in both energy channels. In conclusion, the observed values of electron density in the coronal part of the arcade did not explain the location of the hard X–ray emission sources H3 and H4.

I suspect that the hard X–ray emission sources above footpoints can be a result of a small convergence of the magnetic lines of force in the legs. Let me consider a magnetic flux tube (leg) with a small convergence of the lines of force. Let r_0 be its radius in the upper part, at $s = s_0$ and B_0 - the magnetic field strengh there (s is the coordinate along the magnetic tube). In the low-density approximation the motion of a particle having pitch angle θ_0 at s_0, is described by the equation:

$$\sin^2\theta/\sin^2\theta_0 = B(s)/B_0 = r_0^2/r^2(s) \quad (1)$$

Let B_1, r_1 be the values of B and r at $s = s_1$, where the pitch angle achieves the value $\theta = 90^\circ$ (a magnetic mirror for the particle), then:

$$r_1/r_0 \equiv \sin\theta_0 \quad (2)$$

Now let me assume that directions of particle motions are random (isotropic) at $s = s_0$, near the flare kernel K. Then

$$f(\theta^*) = \cos\theta^*, \quad (3)$$

where $f(\theta^*)$ is the fraction of particles moving downwards having $\theta_0 > \theta^*$.

Let me now assume a very small convergence of the magnetic lines, say $r_1/r_0 = 0.9$. From Eq. (2) we obtain: $\theta_0 = 64^\circ$ and from Eq. (3): $f(\theta^* = 64^\circ) = 0.44$.

The main point of this consideration is that in the case of low plasma density, a very small convergence of the magnetic lines of force causes very significant effects of particle mirroring. And since the particles (electrons) remain for a relatively longer time near their magnetic mirrors, the hard X–ray bremsstrahlung emission will be significantly enhanced there.

Soft X–ray images like those in Fig. 1 suggest that a small convergence of the magnetic lines of force actually occurs in many cases of the flare legs. This has been also confirmed by inspection of the legs of Hα loops for other flares (e.g. Švestka 1976, Fig. 88; Akimov et al. 1996). The effect of magnetic mirroring to explain the observed differences for the hard X–ray double sources located in the footpoints was also suggested by Sakao (1994) for several flaring loops analysed by him. The conclusions of Sakao get strong support from microwave observations (Kundu et al. 1995).

5.3. The impulsive soft X–ray brightenings

Previous reports (Strong et al. 1994; Hudson et al. 1994) emphasized the good spatial agreement between the impulsive soft X–ray brightenings and the hard X–ray emission sources. The 28 June 1992, 14:24 UT flare did not support this result. In some legs (6 and 7) where I observed the impulsive soft X–ray brightenings I did not identify any hard X–ray emission. In other legs (2+3, 4 and 5) the hard X–ray emission sources were several thousand kilometers above the places of impulsive soft X–ray brightenings. Only in the case of the footpoint F1 was an agreement between the impulsive soft X–ray brightening and the hard X–ray emission was seen.

The reported disagreement can be explained by a low flux of high-energy non-thermal electrons and the magnetic field convergence. A majority of non-thermal electrons produced in the loop-top sources was mirrored in those parts of the arcade where we observed other hard X–ray emission sources. A fraction of the non-thermal electrons must have reached the footpoints as evidenced by the impulsive soft X–ray brightenings in Fig. 2b. However, with the exception of the footpoint F1, the bremsstrahlung of non-thermal electrons was not seen in the HXT images.

Finally, the observations of the impulsive soft X–ray brightenings together with the observations of the low-lying hard X–ray emission sources give an unique opportunity to investigate a morphology of precipitated non-thermal electrons in more detailed and complementary way.

6. Conclusions

The 28 June 1992, 14:24 UT arcade flare offers an unusual opportunity to investigate a relationship between the impulsive soft X–ray brightenings and the hard X–ray emission sources. My basic conclusions can be summarized as follows:

1. The morphology of the arcade flare is more complicated than in the case of the single-loop flare. I found evidence of simultanous energy release at two separated places in the top of the arcade and energy distribution along at least seven legs in two forms: non-thermal electron beams and thermal conduction.
2. Simultanous energy release in several places seems to be a rule for the arcade flares (Tomczak 1994; Jakimiec et al. 1996). In the case of the 28 June 1992, 14:24 UT flare the hard X–ray emission loop-top sources had different observational features; in particular, the weaker source had the harder spectrum. In spite of some differences a connection between both places of the energy release was evident.
3. The hard X–ray emission sources above the footpoints were the result of the magnetic field convergence. Magnetic mirroring was responsible for the shift of the places of the precipitation of non-thermal electrons to the higher parts of the legs of the arcade. Only a fraction of non-thermal electrons passed deeper and produced the impulsive soft X–ray brightenings.
4. The observations of the impulsive soft X–ray brightenings are an additional source of information about places of the precipitation of non-thermal electrons. The SXT observations offer better spatial resolution than the HXT images and are especially useful when a weak stream of non-thermal

electrons produces hard X–ray emission that cannot be detected by the HXT telescope.

5. From the time evolution of the moments of the impusive soft X–ray brightenings I estimated the velocity of the chromospheric evaporation. Derived values 460–750 km s^{-1} are consistent with spectral observations from the Bragg Crystal Spectrometer (e.g. Bentley et al. 1994), but greater than results of standard theoretical loop model (e.g. Fisher et al. 1985; Reale & Peres 1995).

Acknowledgements. I acknowledge the really hard work and dedication of the whole *Yohkoh* Team, which has made this research possible. I would like to express my gratitude to Prof. J. Jakimiec for frequent discussions and fruitful advice. I thank also Dr. R. D. Bentley for the installation of the Yohkoh software and Dr. A. Fludra for discussions and comments on the manuscript. This work was supported by the KBN grant No. 2 P304 023 04. The collaboration with the British scientists was supported by the British Council / KBN grant WAR/992/057.

References

Acton, L. W., Feldman, U., Bruner, M. E., et al. 1992, PASJ 44, L71
Akimov, V. V., Ambrož, P., Belov, A. V., et al. 1996, Sol. Phys. 166, 107
Bentley, R. D., Doschek, G. A., Simnett, G. M., et al. 1994, ApJ 421, L55
Feldman, U., Seely, J. F., Doschek, G. A., et al. 1995, ApJ 446, 860
Fisher, G. H., Canfield, R. C., & McClymont, A. N. 1985, ApJ 289, 414
Fishman, G. J. et al. 1989, in: Proc. of the GRO Science Workshop, ed. W. N. Johnson (Greenbelt: NASA/GSFC), p. 2
Hara, H., Tsuneta, T., Lemen, J. R., Acton, L. W., & McTiernan, J. M. 1992, PASJ 44, L135
Hudson, H. S. 1994, in: Proc. of Kofu Symposium, eds. S. Enome & T. Hirayama, NRO Report No. 360, p. 1
Hudson, H. S., Strong, K. T., Dennis, B. R., et al. 1994, ApJ 422, L25
Jakimiec, J. 1990, Adv. Space Res. Vol. 10 No. 9, 109
Jakimiec, J. 1991, paper presented to the XIV Consultation on Solar Physics, Karpacz, Poland, in press
Jakimiec, J., & Fludra, A. 1991, Adv. Space Res. Vol. 11 No. 5, 99
Jakimiec, J. et al. 1994, paper presented to the COSPAR Symposium E2.2, Hamburg, Germany, COSPAR'94 Book of Abstracts, p. 249
Jakimiec, J., Fludra, A., Tomczak, M. & Falewicz, R. 1996, in preparetion
Kosugi, T., Makishima, K., Murakami, T., et al. 1991, Sol. Phys. 136, 17
Kosugi, T. 1994, in: Proc. of Kofu Symposium, eds. S. Enome & T. Hirayama, NRO Report No. 360, p. 11
Kosugi, T., Sakao, T., Masuda, S., et al. 1994, in: Proc. of Kofu Symposium, eds. S. Enome & T. Hirayama, NRO Report No. 360, p. 127
Kundu, M. R., Nitta, N., White, S. M., et al. 1995, ApJ 454, 522
Masuda, S. 1994, PhD thesis, University of Tokyo
Morrison, M. D. 1994, Yohkoh Analysis Guide, Lockheed Palo Alto Research Laboratory
Ogawara, Y., Takano, T., Kato, T., et al. 1991, Sol. Phys. 136, 1
Reale, F., & Peres, G. 1995, A&A 299, 225
Sakao, T. 1994, PhD thesis, University of Tokyo
Strong, K. T., Hudson, H. S., & Dennis, B. R. 1994, in: X-Ray Solar Physics from Yohkoh, eds. Y. Uchida, K. Shibata, T. Watanabe, & H. Hudson, Universal Academy Press (Tokyo), p. 65
Švestka, Z. 1976, Solar Flares (Dordrecht: Reidel)
Tomczak, M. 1994, PhD thesis, University of Wroclaw
Tsuneta, S., Acton, L. W., Bruner, M. E., et al. 1991, Sol. Phys. 136, 37
Uchida, Y. 1995, Adv. Space Res. Vol. 17 No. 4/5, 19

This article was processed by the author using Springer-Verlag LaTeX A&A style file *L-AA* version 3.